


ORIGINAL RESEARCH

Open Access



Predicting [^{177}Lu]Lu-HA-DOTATATE kidney and tumor accumulation based on [^{68}Ga]Ga-HA-DOTATATE diagnostic imaging using semi-physiological population pharmacokinetic modeling

Hinke Siebinga^{1,2,3*} , Berlinda J. de Wit-van der Veen², Jos H. Beijnen¹, Marcel P. M. Stokkel², Thomas P. C. Dorlo^{1,4}, Alwin D. R. Huitema^{1,5,6} and Jeroen J. M. A. Hendriks^{1,2}

*Correspondence:
h.siebinga@nki.nl

¹ Department of Pharmacy and Pharmacology, The Netherlands Cancer Institute, Plesmanlaan 121, 1066 CX Amsterdam, The Netherlands

² Department of Nuclear Medicine, The Netherlands Cancer Institute, Amsterdam, The Netherlands

³ Graduate School of Life Sciences, Utrecht University, Utrecht, The Netherlands

⁴ Department of Pharmacy, Uppsala University, Uppsala, Sweden

⁵ Department of Clinical Pharmacy, University Medical Center Utrecht, Utrecht University, Utrecht, The Netherlands

⁶ Department of Pharmacology, Princess Máxima Center for Pediatric Oncology, Utrecht, The Netherlands

Abstract

Background: Prediction of [^{177}Lu]Lu-HA-DOTATATE kidney and tumor uptake based on diagnostic [^{68}Ga]Ga-HA-DOTATATE imaging would be a crucial step for precision dosing of [^{177}Lu]Lu-HA-DOTATATE. In this study, the population pharmacokinetic (PK) differences between [^{177}Lu]Lu-HA-DOTATATE and [^{68}Ga]Ga-HA-DOTATATE were assessed and subsequently [^{177}Lu]Lu-HA-DOTATATE was predicted based on [^{68}Ga]Ga-HA-DOTATATE imaging.

Methods: A semi-physiological nonlinear mixed-effects model was developed for [^{68}Ga]Ga-HA-DOTATATE and [^{177}Lu]Lu-HA-DOTATATE, including six compartments (representing blood, spleen, kidney, tumor lesions, other somatostatin receptor expressing organs and a lumped rest compartment). Model parameters were fixed based on a previously developed physiologically based pharmacokinetic model for [^{68}Ga]Ga-HA-DOTATATE. For [^{177}Lu]Lu-HA-DOTATATE, PK parameters were based on literature values or estimated based on scan data (four time points post-injection) from nine patients. Finally, individual [^{177}Lu]Lu-HA-DOTATATE uptake into tumors and kidneys was predicted based on individual [^{68}Ga]Ga-HA-DOTATATE scan data using Bayesian estimates. Predictions were evaluated compared to observed data using a relative prediction error (RPE) for both area under the curve (AUC) and absorbed dose. Lastly, to assess the predictive value of diagnostic imaging to predict therapeutic exposure, individual prediction RPEs (using Bayesian estimation) were compared to those from population predictions (using the population model).

Results: Population uptake rate parameters for spleen, kidney and tumors differed by a 0.29-fold (15% relative standard error (RSE)), 0.49-fold (15% RSE) and 1.43-fold (14% RSE), respectively, for [^{177}Lu]Lu-HA-DOTATATE compared to [^{68}Ga]Ga-HA-DOTATATE. Model predictions adequately described observed data in kidney and tumors for both peptides (based on visual inspection of goodness-of-fit plots). Individual predictions of tumor uptake were better (RPE AUC -40 to 28%) compared to kidney

predictions (RPE AUC –53 to 41%). Absorbed dose predictions were less predictive for both tumor and kidneys (RPE tumor and kidney –51 to 44% and –58 to 82%, respectively). For most patients, [¹⁷⁷Lu]Lu-HA-DOTATATE tumor accumulation predictions based on individual PK parameters estimated from diagnostic imaging outperformed predictions based on population parameters.

Conclusion: Our semi-physiological PK model indicated clear differences in PK parameters for [⁶⁸Ga]Ga-HA-DOTATATE and [¹⁷⁷Lu]Lu-HA-DOTATATE. Diagnostic images provided additional information to individually predict [¹⁷⁷Lu]Lu-HA-DOTATATE tumor uptake compared to using a population approach. In addition, individual predictions indicated that many aspects, apart from PK differences, play a part in predicting [¹⁷⁷Lu]Lu-HA-DOTATATE distribution.

Keywords: [⁶⁸Ga]Ga-HA-DOTATATE, [¹⁷⁷Lu]Lu-HA-DOTATATE, Theranostics, PRRT, NLMEM, Uptake prediction, Precision medicine

Introduction

Somatostatin analogue (SSA)-based peptide receptor radionuclide therapy (PRRT) is increasingly used for the treatment of metastasized well-differentiated neuroendocrine tumors (NETs) [1]. As the outcome after PRRT varies among patients, selection of those suitable for therapy is guided by SSA-based molecular imaging to assess tumor load and expression of somatostatin receptors (SSTR) for individual lesions [2]. This theranostic approach has the benefit that pre-therapeutic imaging may predict treatment response and lead to more effective personalized treatment dosages [3, 4]. Interestingly, in case of NET, both organ uptake and tumor targeting have shown quite profound differences between diagnostic and peri-therapeutic imaging in the clinical setting [5–10]. As PRRT evolves toward a more dosimetry-driven treatment [11–14], these differences will become relevant and identification of physiological or pharmacokinetic (PK) factors that influence accumulation profiles are gaining importance.

Lutetium-177 ([¹⁷⁷Lu]Lu-)DOTATATE shows a high inter-patient variability for both organ and tumor uptake [15] and this variability is an important rationale to pursue future personalized treatment planning based on (expected) absorbed doses. To introduce image-guided individualized dosing, the applicability of diagnostic single-time-point Gallium-68 ([⁶⁸Ga]Ga-)DOTATATE imaging to predict the [¹⁷⁷Lu]Lu-DOTATATE accumulation profiles needs to be studied. Direct extrapolation of diagnostic uptake profiles is not straightforward, since factors such as image noise, patients' hydration status and timing of imaging post-injection all differ and are known to impact visualization of the distribution [16]. As was suggested by Velikyan et al. [17], kinetic modeling could be used to enhance extrapolation of [⁶⁸Ga]Ga-DOTATATE early imaging time points to predict absorbed [¹⁷⁷Lu]Lu-DOTATATE doses to tumors and organs.

Population PK models are a suitable approach to investigate PK parameters of both radiopharmaceuticals and their variability within a population [18, 19]. Such population PK modeling approaches are the golden standard in drug development and research of non-radiopharmaceuticals and are a proven tool to handle sparse data sampling, which is an advantage when applying this approach to nuclear imaging data [20]. A population PK model describes population-based radioactivity–time profiles (or time–activity curves (TACs)), which, combined with individual data, will give insights in how a specific patient differs from the population estimate. We hypothesize that the individual

difference from these population estimates is rather similar for [^{68}Ga]Ga- and [^{177}Lu]Lu-DOTATATE and is mainly driven by an individual's physiology (e.g., SSTR expression and tumor physiology). Therefore, relevant physiological aspects need to be included in the developed population PK models (i.e., using a semi-physiological approach). Still, in this case, a physiologically based pharmacokinetic (PBPK) approach was not preferable, since insights in population trends were required to individually estimate deviation from the typical population. Considering that radiopharmaceutical-related variables (e.g., injected activity and/or peptide amounts, clearance and receptor-mediated uptake) are already included in a population model, [^{68}Ga]Ga-DOTATATE scan observations could be used to predict individual PK parameters of [^{177}Lu]Lu-DOTATATE.

As a first step toward population PK-informed predictions, actual differences in population PK parameters between both theranostic agents have to be determined (i.e., ^{68}Ga - and ^{177}Lu -labeled high-affinity DOTATATE (HA-DOTATATE) in our hospital [21]). Hence, the initial aim of this study was to assess population PK differences between [^{68}Ga]Ga-HA-DOTATATE and [^{177}Lu]Lu-HA-DOTATATE using a semi-physiological population PK modeling approach. Subsequently, these models are then used to individually predict [^{177}Lu]Lu-HA-DOTATATE kidney (organ at risk) and tumor (target tissue) uptake based on single-time-point imaging with [^{68}Ga]Ga-HA-DOTATATE.

Methods

Patient population and imaging data

This study included data from ten patients with NETs who had received [^{68}Ga]Ga-HA-DOTATATE PET/CT within six months prior to [^{177}Lu]Lu-HA-DOTATATE treatment [22]. The study was approved by the Institutional Review Board of the Netherlands Cancer Institute (IRBd21187) and informed consent was obtained via institutional procedures from all individual participants included in the study.

Diagnostic PET/CT imaging was performed at ~45 min post-injection of ~100 MBq [^{68}Ga]Ga-HA-DOTATATE. All patients received ~7.4 GBq [^{177}Lu]Lu-HA-DOTATATE followed by post-administration imaging, including planar scintigraphy at 0.5, 4, 24 and 72 h post-injection and SPECT/CT at 24 h post-injection. [^{68}Ga]Ga-HA-DOTATATE and [^{177}Lu]Lu-HA-DOTATATE were prepared in house according to previously described methods [23, 24]. Patient selection, data acquisition and data analysis were described previously [22]. Individual accumulation data for spleen, kidneys and tumor lesions were available, whereas no blood samples were drawn. For tumors, only lesions with a diameter >2 cm and a maximum of five segmented lesions of which two per organ system per patient (i.e., target tumors) were included for model development. To exclude potential treatment effects on whole-body distribution, only the first cycle [^{177}Lu]Lu-HA-DOTATATE was included for model development in this study. All tumor volumes were determined based on PET/CT imaging using IntelliSpace Portal (Philips Healthcare, The Netherlands) with a semi-automatic threshold segmentation method of 50% SUV_{max} [25]. Decay corrected peptide concentrations ($\mu\text{g}/\text{L}$) were used for model development and evaluation, which were calculated based on the measured radioactivity per volume and the administered specific activities ($\text{MBq}/\mu\text{g}$) (using total administered peptide amounts).

Model development

In order to describe and compare differences in (population) PK between $[^{68}\text{Ga}]\text{Ga-HA-DOTATATE}$ and $[^{177}\text{Lu}]\text{Lu-HA-DOTATATE}$, two semi-physiological nonlinear mixed-effects models (NLMEMs) with a similar model structure were developed. Using this approach, differences in population PK parameters between both radiopharmaceuticals were determined. An overview of the workflow is provided in Fig. 1. First, a population PK model of $[^{68}\text{Ga}]\text{Ga-HA-DOTATATE}$ was developed fully informed by a previously developed PBPK model [26]. Subsequently, the model structure was applied to $[^{177}\text{Lu}]\text{Lu-HA-DOTATATE}$ and parameters describing differences between both radiopharmaceuticals were estimated. Finally, both developed models were used to predict $[^{177}\text{Lu}]\text{Lu-HA-DOTATATE}$ PK based on $[^{68}\text{Ga}]\text{Ga-HA-DOTATATE}$ observations.

Semi-physiological PK model $[^{68}\text{Ga}]\text{Ga-HA-DOTATATE}$

The first step of our approach was to develop a semi-physiological model for $[^{68}\text{Ga}]\text{Ga-HA-DOTATATE}$. Structural model development was informed based on a previously published PBPK model [26], where compartments were lumped based on their SSTR-expressing nature. This resulted in a six-compartment structural model, where compartments one to six represented the blood compartment, spleen, kidney, tumor lesions, other SSTR-expressing organs and a lumped rest compartment, respectively. Compartment five consisted of the lungs, pancreas, stomach, thyroid and liver. The full model structure is presented in Fig. 2. Structural model parameters were based on estimates from a previously published PBPK model [26]. Organ volumes were fixed for all patients and derived from the ICRP Publication 89 adult human model [27]. The tumor compartment volume was based on individual measured tumor volumes and consisted of the sum of volumes of all segmented tumors (based on [22]).

Uptake into organs and tumor occurs by internalization of the radiopharmaceutical after SSTR receptor binding [28], which was included for all SSTR-expressing

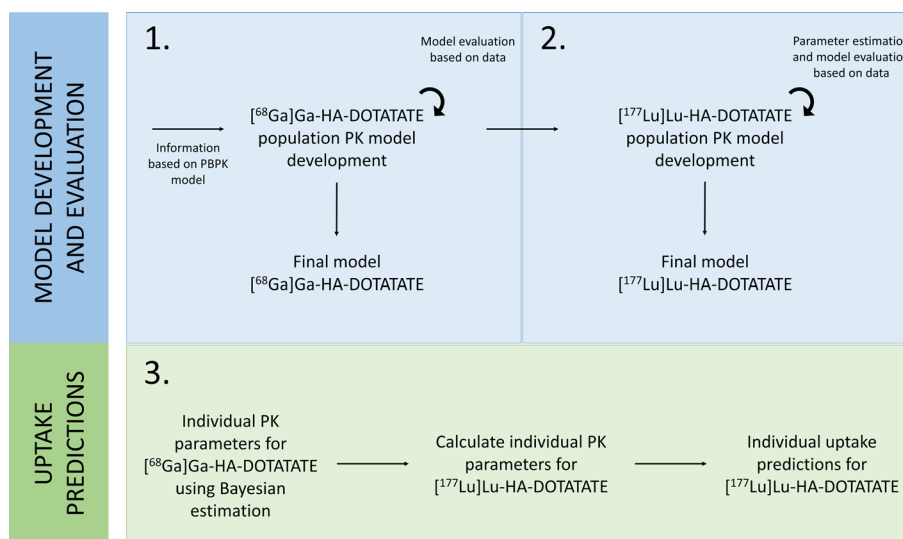


Fig. 1 Overview of the study workflow including model development and evaluation for $[^{68}\text{Ga}]\text{Ga-HA-DOTATATE}$ and $[^{177}\text{Lu}]\text{Lu-HA-DOTATATE}$ and individual uptake predictions for $[^{177}\text{Lu}]\text{Lu-HA-DOTATATE}$

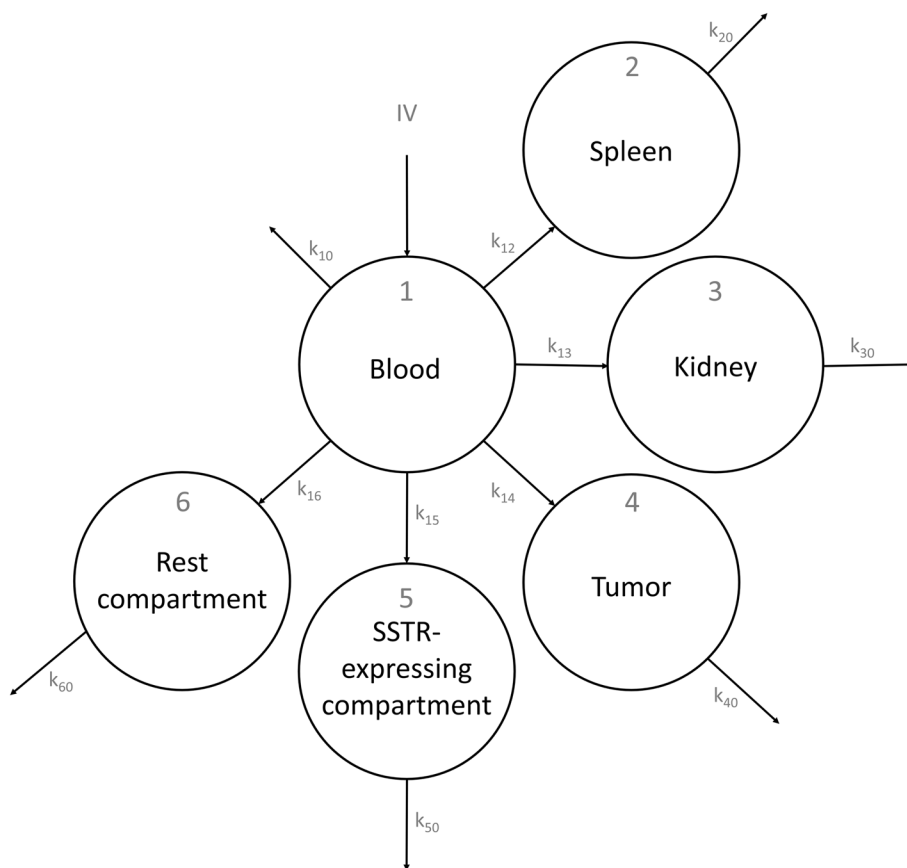


Fig. 2 Overview of the model six-compartment structure for both the $[^{68}\text{Ga}]\text{Ga-HA-DOTATATE}$ and $[^{177}\text{Lu}]\text{Lu-HA-DOTATATE}$ models

compartments (two, three, four and five). Degradation from all compartments was described by a degradation rate constant (k_{20} , k_{30} , k_{40} , k_{50} and k_{60}) and was fixed to 0.01 h^{-1} based on previously published PBPK models [26, 29, 30]. Uptake was modeled using a maximal binding capacity (B_{MAX}) model (Eq. 1), where occupancy of the receptor was taken into account and free binding sites decreased with uptake of each molecule into that compartment (i.e., the amount of radiopharmaceutical that was already internalized into the compartment). B_{MAX} amounts were calculated based on the compartment volume, thus, for compartment four, larger tumors had a higher maximal SSTR binding capacity. In addition, fractions bound to plasma proteins were taken into account and only unbound molecules were available for uptake into compartments.

$$\frac{dA}{dt} = k_{in} * fu * A_{\text{blood}} * \left(1 - \frac{A}{B_{\text{MAX}}}\right) - k_{out} * A \tag{1}$$

where k_{in} and k_{out} represent the rate constants into a specific compartment, fu is the unbound fraction of the radiopharmaceutical in the blood compartment, A_{blood} and A represent the compound amounts in the blood and target compartment, respectively, and B_{MAX} is the maximum binding capacity in the target compartment (i.e., SSTR receptor expression).

The stochastic or statistical model accounted for inter-individual variability (IIV) and residual unexplained variability. For $[^{68}\text{Ga}]\text{Ga-HA-DOTATATE}$, IIV was added to uptake rate parameters. IIV was fixed based on assumed population variability, using information from ranges included in the previously developed PBPK model, assumed variability in uptake in organs and tumors based on clinical observations and estimated IIV in previously published population PK models for radiolabeled SSAs [26, 31, 32]. IIV was modeled using an exponential distribution according to Eq. 2, while a proportional error model described the residual error according to Eq. 3.

$$P_i = P_{\text{pop}} * e^{\eta_i} \tag{2}$$

$$C_{\text{obs},ij} = C_{\text{pred},ij} * (1 + \varepsilon_{p,ij}) \tag{3}$$

where P_i represents the individual PK parameter, P_{pop} represents the population PK parameter, and η_i represents the IIV effect for the i th individual with mean 0 and variance ω^2 . C_{obs} represents the observed concentration and C_{pred} the predicted concentration for the i th individual and the j th measurement, and ε_p the proportional error with mean 0 and variance σ^2 for the i th individual and the j th measurement.

Factors known to affect PK parameters were added to the model a priori, since model development was based on fixed parameters rather than estimated based on data. Radiopharmaceutical distribution in NET patients might be impacted by a tumor sink effect, which reflects a reduced uptake in healthy tissues due to a high burden of disease [33]. Therefore, the tumor sink effect was included in the model following Eq. 4, where the extent of this effect was based on previous PBPK simulations [26]. In addition, a larger tumor volume is expected to increase tumor uptake, as was also shown for $[^{68}\text{Ga}]\text{Ga-PSMA-11}$ [34]. Therefore, individual tumor burden was added as a structural effect to uptake into tumor lesions (k_{14}), using a power equation (see Eq. 5), so that patients with a high tumor volume will have an increased tumor uptake compared to the typical population.

$$k_{12,\text{cov}} = k_{12,\text{pop}} * e^{0.4 * (-V_{\text{tumor total},i})} \tag{4}$$

$$k_{14,\text{cov}} = k_{14,\text{pop}} * \left(\frac{V_{\text{tumor cmt},i}}{V_{\text{tumor cmt,median}}} \right)^{\text{eff}} \tag{5}$$

where $k_{12,\text{pop}}$ and $k_{14,\text{pop}}$ represent the population uptake rates for spleen (compartment two) and tumor (compartment four), respectively, $V_{\text{tumor total},i}$ represents an individual's total tumor volume, $V_{\text{tumor cmt},i}$ represents an individual's tumor volume of all segmented tumors (representing compartment 4), $V_{\text{tumor cmt,median}}$ was the median tumor volume of the tumor compartment and eff represents the structural effect of tumor volume on k_{14} .

A bottom-up approach was used for $[^{68}\text{Ga}]\text{Ga-HA-DOTATATE}$ model development and patient imaging data were only used for model evaluation. All model parameters were fixed, since our single-time-point data were limited to estimate PK parameters, and most parameters were based on the previously developed PBPK model [26]. The fraction of $[^{68}\text{Ga}]\text{Ga-HA-DOTATATE}$ bound to plasma proteins, renal excretion and structural effect of tumor volume on k_{14} (see Eq. 5) were fixed to 0.69 and 0.25 h^{-1} and 1,

respectively [26]. Eventual concentration over time predictions based on the semi-physiological population model for $[^{68}\text{Ga}]\text{Ga-HA-DOTATATE}$ were visually evaluated using observed concentration–time data.

$[^{177}\text{Lu}]\text{Lu-HA-DOTATATE}$ parameter estimation and model evaluation

The second step was to develop the $[^{177}\text{Lu}]\text{Lu-HA-DOTATATE}$ model, and for this all initial model parameters were based on the final model for $[^{68}\text{Ga}]\text{Ga-HA-DOTATATE}$. Most parameters were assumed similar for both agents. Renal excretion is known to be increased for $[^{177}\text{Lu}]\text{Lu-HA-DOTATATE}$ compared to $[^{68}\text{Ga}]\text{Ga-HA-DOTATATE}$ and, therefore, k_{10} was fixed to 0.575 h^{-1} based on a clearance value of 2.3 L/h as was estimated by Puzskiel et al. [31]. Administration of an amino acid solution during therapy compared to no kidney protection during diagnostic imaging was taken into account, since this used renal excretion rate was estimated for patients that received an amino acid solution during administration of $[^{177}\text{Lu}]\text{Lu-DOTATATE}$. Fraction unbound in plasma was fixed to 0.57 [35]. Uptake into spleen, kidney and tumor as well as degradation from tumor were expected to differ for $[^{177}\text{Lu}]\text{Lu-HA-DOTATATE}$; thus, the PK parameters for k_{12} , k_{13} , k_{14} , k_{40} and the structural effect of tumor volume on k_{14} (see Eq. 5) were sequentially estimated using patient imaging data (on four time points post-injection). PK parameters for $[^{177}\text{Lu}]\text{Lu-HA-DOTATATE}$ were estimated as fold differences compared to $[^{68}\text{Ga}]\text{Ga-HA-DOTATATE}$ parameters, to enable easy comparison of final population PK parameters between both theranostic agents. Kidney data from each first imaging time point (at $\sim 1\text{ h}$ post-injection) were excluded for parameter estimation, because these observations were assumed to mainly represent urine activity rather than intracellular uptake. IIV for $[^{177}\text{Lu}]\text{Lu-HA-DOTATATE}$ was added to receptor expressions rather than k_{in} values (as was the case for $[^{68}\text{Ga}]\text{Ga-HA-DOTATATE}$). The rationale that receptor expressions were assumed to describe the inter-individual uptake differences was based on the differences in administered peptide amounts between the radiopharmaceuticals. For $[^{68}\text{Ga}]\text{Ga-HA-DOTATATE}$, a very low amount of peptide is administered and receptors are not close to full occupancy, while for $[^{177}\text{Lu}]\text{Lu-HA-DOTATATE}$ (with an almost 30-fold higher administered peptide amount) uptake is mainly reliant on receptor density. A low impact of receptor expression on total uptake for $[^{68}\text{Ga}]\text{Ga-HA-DOTATATE}$ was also shown by the sensitivity analyses in our previously published PBPK models [26, 36]. Final model performance for $[^{177}\text{Lu}]\text{Lu-HA-DOTATATE}$ was evaluated based on visual inspection of predictions compared to observations and clinical plausibility of estimated parameter values was assessed.

Individual $[^{177}\text{Lu}]\text{Lu-HA-DOTATATE}$ predictions using Bayesian estimation

The third and last step consisted of individual $[^{177}\text{Lu}]\text{Lu-HA-DOTATATE}$ uptake prediction informed by diagnostic imaging. Individual PK parameters for $[^{68}\text{Ga}]\text{Ga-HA-DOTATATE}$ were generated using Maximum a Posteriori Bayesian estimation (POSTHOC option of NONMEM, about which more information is available elsewhere [37]). Subsequently, these Bayesian estimates were used to predict individual parameters for $[^{177}\text{Lu}]\text{Lu-HA-DOTATATE}$ based on the established differences between PK parameters of both radiopharmaceuticals. The predicted individual $[^{177}\text{Lu}]\text{Lu-HA-DOTATATE}$ PK parameters, combined with individual administered dosing and covariate

information, were then used to predict [¹⁷⁷Lu]Lu-HA-DOTATATE concentration–time curves for all compartments.

Absorbed doses for kidney and tumor were determined to evaluate the predicted energy deposited in the irradiated tissue. For this, time-integrated activity (TIA) (MBq*h) was determined using calculated AUCs (μg*h/L) in kidney and tumors, organ and tumor volumes (L) and injected specific activity (MBq/μg). The TIA was extrapolated to infinite time based on the calculated excretion rate per individual. After this, absorbed doses were calculated following the Medical Internal Radiation Dose (MIRD) formalism [38]. Organ weights that were used for absorbed dose calculations were based on the ICRP Publication 89 adult male human model and corresponding S values were derived from IDAC-Dose 2.1 [27, 39]. For tumors, individual tumor volumes and a tissue density of 1.05 g/cm³ were used to determine the corresponding S value.

Evaluation of predictions

Predictive performance was evaluated by determining the relative prediction error (RPE) of area under the curves (AUCs) (time interval from 0 to time of the last measurement) for kidney and tumor, where predicted AUCs were compared to observed AUCs (based on four post-administration images per patient) following Eq. 6.

$$RPE = \frac{AUC_{pred} - AUC_{obs}}{AUC_{obs}} * 100\% \quad (6)$$

where AUC_{pred} and AUC_{obs} represent the predicted and observed AUC, respectively.

Predictions for [¹⁷⁷Lu]Lu-HA-DOTATATE PK based on Bayesian estimates were compared to predictions based on the typical values in the population (i.e., the final population PK parameters, not taking [⁶⁸Ga]Ga-HA-DOTATATE observations into account). For this, RPEs of both approaches were compared and a lower RPE was determined a better prediction.

Software

Model development was performed in NONMEM (version 7.5; ICON Development Solutions, Ellicott City, MD, USA), where in case of parameter estimation the first-order conditional estimation method with interaction (FOCE-I) was used. R (version 4.1.3) was used for data processing, model evaluation by visualization of goodness-of-fit (GOF) plots and final uptake predictions.

Results

Patients and data

Data from ten patients with NETs who received a diagnostic [⁶⁸Ga]Ga-HA-DOTATATE PET/CT and PRRT with [¹⁷⁷Lu]Lu-HA-DOTATATE were included. Patient one was excluded, since tumor lesions were not suitable for accurate quantitative analysis as diameters were less than two cm. For patient two, kidney data were excluded from analysis because only one kidney was available for quantitative analysis. Patient characteristics are shown in Table 1. Median (range) administered peptide amounts were 5.23 μg (3.01–9.64 μg) and 151 μg (132–178 μg) for [⁶⁸Ga]Ga-HA-DOTATATE

and [¹⁷⁷Lu]Lu-HA-DOTATATE, respectively. Median (range) tumor volume of target tumors (representing the tumor compartment) was 80.0 mL (7.81–212 mL), while median (range) total tumor volume was 283 mL (22.4–644 mL). Individual [⁶⁸Ga]Ga-HA-DOTATATE and [¹⁷⁷Lu]Lu-HA-DOTATATE peptide concentration–time curves (based on imaging data) for spleen, kidney and tumor are shown in Fig. 3.

Table 1 Patient characteristics

Characteristic	Median (range) or number (%)
Sex	
Male (n)	4 (44%)
Female (n)	5 (56%)
Age (years)	70 (44–76)
Weight (kg)	75.0 (55.0–108)
Height (cm)	174 (160–189)
Creatinine clearance (mL/min)	68.8 (53.6–111)
Tumor volume of target tumors (representing the tumor compartment) ^a (mL)	80.0 (7.81–212)
Total tumor volume ^b (mL)	283 (22.4–644)
Injected radioactivity	
[⁶⁸ Ga]Ga-HA-DOTATATE (MBq)	96.0 (75.6–102)
[¹⁷⁷ Lu]Lu-HA-DOTATATE (MBq)	7271 (7176–7613)
Injected peptide amount	
[⁶⁸ Ga]Ga-HA-DOTATATE (μg)	5.23 (3.01–9.64)
[¹⁷⁷ Lu]Lu-HA-DOTATATE (μg)	151 (132–178)

^aTarget tumors represent lesions with a diameter > 2 cm and a maximum of five segmented lesions of which two per organ system per patient

^bSum of tumor volumes of all tumors (including target tumors)

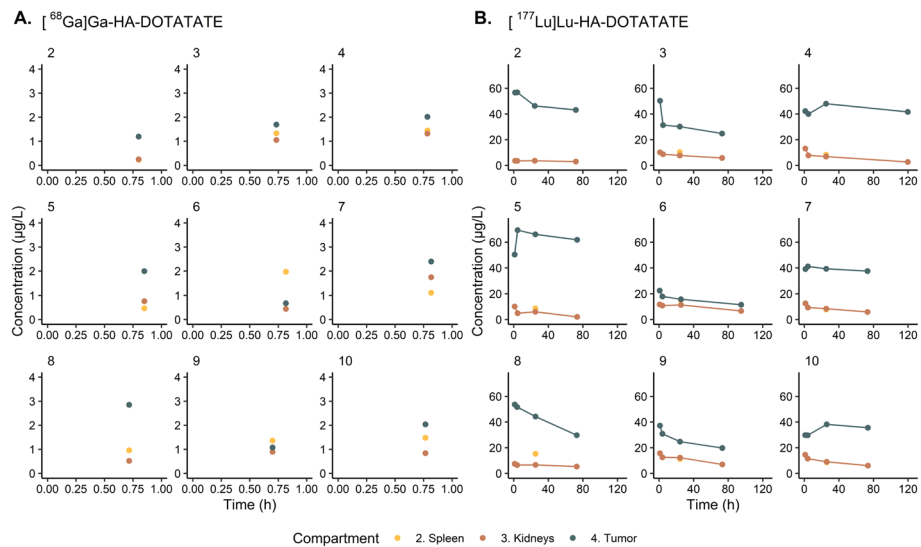


Fig. 3 Individually observed concentrations (μg/L) of **A** [⁶⁸Ga]Ga-HA-DOTATATE and **B** [¹⁷⁷Lu]Lu-HA-DOTATATE in the spleen, kidney and tumors (stratified for patients 2 to 10)

Semi-physiological PK model

All PK parameters for the $[^{68}\text{Ga}]\text{Ga-HA-DOTATATE}$ and $[^{177}\text{Lu}]\text{Lu-HA-DOTATATE}$ models are shown in Table 2. Population uptake rate parameters (k_{in}) for spleen, kidney and tumors differed by a 0.29- (15% relative standard error (RSE)), 0.49- (15% RSE) and 1.43-fold (14% RSE), respectively, for $[^{177}\text{Lu}]\text{Lu-HA-DOTATATE}$ compared to $[^{68}\text{Ga}]\text{Ga-HA-DOTATATE}$. Model fits adequately described observed data in kidney and tumors for both peptides. GOF plots of the $[^{68}\text{Ga}]\text{Ga-HA-DOTATATE}$ and $[^{177}\text{Lu}]\text{Lu-HA-DOTATATE}$

Table 2 Overview of final model parameter differences for $[^{68}\text{Ga}]\text{Ga-HA-DOTATATE}$ and $[^{177}\text{Lu}]\text{Lu-HA-DOTATATE}$, where compartments represent blood (1), spleen (2), kidney (3), tumor (4), a SSTR-expressing (5) and rest (6) compartment

	Parameter values (RSE% provided for estimated values*)	
	$[^{68}\text{Ga}]\text{Ga-HA-DOTATATE}$	$[^{177}\text{Lu}]\text{Lu-HA-DOTATATE}$
Structural parameters		
k_{10} (h^{-1})	0.25	0.575
k_{12} (h^{-1})	0.21	0.0607 (0.29-fold difference (15%))
k_{20} (h^{-1})	0.01	0.01
k_{13} (h^{-1})	0.22	0.107 (0.49-fold difference (15%))
k_{30} (h^{-1})	0.01	0.01
k_{14} (h^{-1})	0.11	0.157 (1.43-fold difference (14%))
k_{40} (h^{-1})	0.01	0.00375 (0.38-fold difference (35%))
k_{15} (h^{-1})	2.5	2.5
k_{50} (h^{-1})	0.01	0.01
k_{16} (h^{-1})	1	1
k_{60} (h^{-1})	0.01	0.01
V1 (L)	4	4
V2 (L)	0.21	0.21
V3 (L)	0.3	0.3
V5 (L)	4	4
V6 (L)	50	50
Fraction unbound in plasma	0.69	0.57
B_{MAX} compartment 2 (nmol/L)	16.7	16.7
B_{MAX} compartment 3 (nmol/L)	6.7	6.7
B_{MAX} compartment 4 (nmol/L)	30	30
B_{MAX} compartment 5 (nmol/L)	2.4	2.4
IIV (CV%)		
k_{10}	31.6%	31.6%
k_{12} or B_{MAX} compartment 2**	50%	50%
k_{13} or B_{MAX} compartment 3**	50%	50%
k_{14} or B_{MAX} compartment 4**	50%	50%
k_{15} or B_{MAX} compartment 5**	31.6%	31.6%
Structural effect		
Tumor volume on k_{14}	1	0.67 (17%)
RUV		
Proportional error (CV%)	31.6%	31.6%

RSEs were obtained from the NONMEM covariance step. The tumor compartment volume parameter (V4) was based on individually measured tumor volumes

B_{MAX} , maximum binding capacity; V, compartment volume; CV%, coefficient of variation; IIV, inter-individual variability; RSE, relative standard error; RUV, residual unexplained variability

*PK parameters for $[^{177}\text{Lu}]\text{Lu-HA-DOTATATE}$ were estimated as a fold difference compared to the parameter for $[^{68}\text{Ga}]\text{Ga-HA-DOTATATE}$

**IIV was added to k parameters for $[^{68}\text{Ga}]\text{Ga-HA-DOTATATE}$, while for $[^{177}\text{Lu}]\text{Lu-HA-DOTATATE}$ IIV was added to B_{MAX}

Table 3 Individual tumor and kidney AUC predictions versus observations for [¹⁷⁷Lu]Lu-HA-DOTATATE, followed by calculated RPEs per patient (ID2–ID10)

AUC _{0-tlast} (mg*h/L)	ID2	ID3	ID4	ID5	ID6	ID7	ID8	ID9	ID10
<i>Tumor</i>									
Observed	3.32	2.09	5.29	4.69	1.38	2.80	2.94	1.76	2.59
Predicted	2.95	2.67	4.05	2.89	0.825	3.06	3.16	1.50	2.60
RPE	−11%	28%	−23%	−38%	−40%	9%	8%	−14%	0%
<i>Kidney</i>									
Observed	–	0.520	0.634	0.334	0.902	0.564	0.443	0.764	0.621
Predicted	–	0.533	0.680	0.469	0.408	0.479	0.410	0.496	0.426
RPE	–	4%	14%	41%	−53%	−12%	−10%	−32%	−32%

AUC_{0-tlast}, area under the curve, calculated from time is 0 to time of the last measurement; RPE, relative prediction error (((predicted – observed)/observed) * 100%)

Table 4 Individual tumor and kidney absorbed dose predictions versus observations for [¹⁷⁷Lu]Lu-HA-DOTATATE, followed by calculated RPEs per patient (ID2–ID10)

Absorbed dose (Gy)	ID2	ID3	ID4	ID5	ID6	ID7	ID8	ID9	ID10
<i>Tumor</i>									
Observed	24.4	14.4	29.3	38.3	8.67	34.4	19.5	12.4	27.7
Predicted	21.3	17.4	19.6	18.7	5.62	25.5	28.1	12.1	21.5
RPE	−13%	21%	−33%	−51%	−35%	−26%	44%	−3%	−23%
<i>Kidney</i>									
Observed	–	3.12	2.21	1.19	5.38	3.92	3.79	4.41	3.71
Predicted	–	2.57	2.57	2.69	2.17	2.26	2.81	2.51	2.75
RPE	–	33%	−18%	21%	82%	−58%	−28%	−34%	−38%

RPE, relative prediction error (((predicted – observed)/observed) * 100%)

Lu-HA-DOTATATE model are shown in Additional file 1: Figures S1 and S2, respectively. In addition, η values were normally distributed.

Maximum receptor occupancy after administration of [¹⁷⁷Lu]Lu-HA-DOTATATE ranged from 39 to 55% for spleen, 71–97% for kidney and 78–100% for tumors and this occupancy decreased over time for all compartments.

Individual [¹⁷⁷Lu]Lu-HA-DOTATATE predictions

Predictions for [¹⁷⁷Lu]Lu-HA-DOTATATE concentration–time curves based on individual Bayesian PK parameter estimates for [⁶⁸Ga]Ga-HA-DOTATATE PK showed reasonably well individual fits for tumors (RPE for AUC in the range of −40 to 28%). Predicted individual kidney concentration–time curves were less accurate, with RPE for AUC between −53 and 41%. Individual AUC prediction versus observation and RPE results for kidney and tumor are shown in Table 3. For absorbed doses, differences between individual predictions and observations were more pronounced (see Table 4), with RPEs for tumor ranging from −51 to 44%, while for kidney this was −58 to 82%. All individual [¹⁷⁷Lu]Lu-HA-DOTATATE predictions and observations are presented in Additional file 1: Figure S3.

Individual RPEs were compared to RPEs based on the final population model estimates for tumors and kidney AUC predictions (see Fig. 4). For tumors, individual predictions

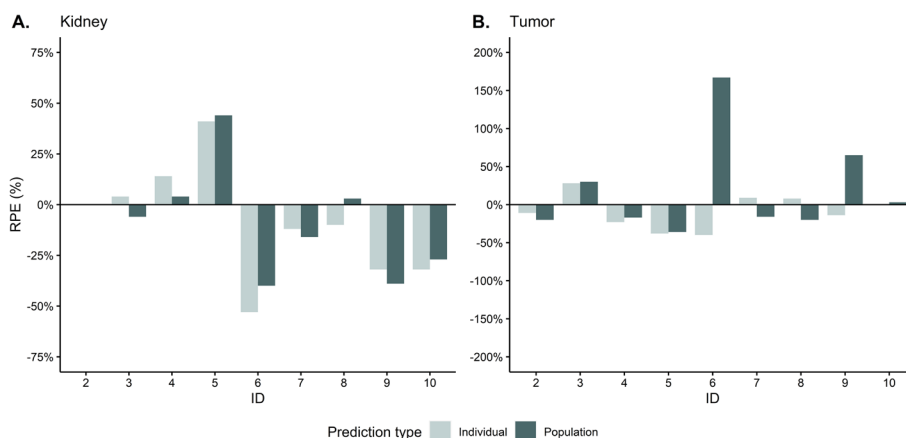


Fig. 4 Comparison of individual and population relative prediction errors (RPEs) for kidney (A) and tumors (B), stratified per individual, based on predicted vs observed area under the curves of [^{177}Lu]Lu-HA-DOTATATE

outperformed population predictions in seven of nine cases. However, for kidney the population predictions seemed to perform better for four of eight patients.

Discussion

A semi-physiological PK model was developed to predict [^{177}Lu]Lu-HA-DOTATATE kidney and tumor uptake based on single-time-point pre-therapeutic PET/CT imaging with [^{68}Ga]Ga-HA-DOTATATE, to pave the way for image-based treatment planning in PRRT. This physiologically informed population PK model provided insights in population trends and allowed individual Bayesian estimation of absorbed doses. This is an advantage compared to conventional PBPK models, where a bottom-up approach is used and variability in individual differences is not identified but needs to be included beforehand (on many different parameters) to describe variability in the data [20]. Moreover, all relevant physiological parameters that could impact radiopharmaceutical distribution or uptake were still included in the model, and the simpler model structure (compared to full PBPK models) enabled straightforward comparison of both radiopharmaceuticals. This provided a first prediction of the PK profiles of both radiopharmaceuticals in NET patients, taking into account relevant system- and drug-specific parameters as well as IIV and structural effects.

Semi-physiological model development

The tumor sink effect (i.e., reduced organ uptake with increasing total tumor volume) was assumed similar for [^{68}Ga]Ga-HA-DOTATATE and [^{177}Lu]Lu-HA-DOTATATE. However, a more profound sink effect due to structural difference might be hypothesized during therapy, since the current study showed that biodistribution of both agents was also different (i.e., [^{177}Lu]Lu-HA-DOTATATE showed a lower spleen and kidney uptake, while tumor uptake rates were higher compared to [^{68}Ga]Ga-HA-DOTATATE). Still, the assumption of the effect being similar (i.e., the effect for an individual being within the same order of magnitude for both agents) seemed most suitable, since we do not have any information based on population data regarding a tumor sink effect during PRRT. For [^{177}Lu]Lu-HA-DOTATATE, the degradation rate in tumors (k_{40}) was estimated

based on data, which resulted in a lower rate (0.00375 h^{-1}) compared to rate constant used for $[^{68}\text{Ga}]\text{Ga-HA-DOTATATE}$ (0.01 h^{-1}). This degradation rate in tumor being different does not per se reflect a difference in degradation between both radiopharmaceuticals, but was the result of the fact that this rate constant for $[^{68}\text{Ga}]\text{Ga-HA-DOTATATE}$ could not be estimated based on a single observation per individual.

Relevance of PK differences

Unfortunately, data regarding radionuclide therapies is often limited with sparse data observations. Still, our approach using a lumped semi-physiological PK model (based on a previously developed PBPK model and literature data) proved that these limited data are still useful for model development (based on fixed parameters) (see Additional file 1: Figures S1 and S2). Model results showed clear differences in uptake rate parameters for spleen, kidney and tumors for $[^{68}\text{Ga}]\text{Ga-HA-DOTATATE}$ compared to $[^{177}\text{Lu}]\text{Lu-HA-DOTATATE}$. The reduced uptake rate in kidney and spleen for $[^{177}\text{Lu}]\text{Lu-HA-DOTATATE}$ was accompanied by increased uptake into the tumor compartment, which was also reflected by an increased uptake rate for tumors (k_{14}). For kidneys, a lower uptake rate was to be expected, since $[^{177}\text{Lu}]\text{Lu-HA-DOTATATE}$ infusion is co-administered with an amino acid solution for renal toxicity prevention. This solution results in less proximal reabsorption and thus kidney uptake is expected to be reduced compared to $[^{68}\text{Ga}]\text{Ga-HA-DOTATATE}$ [40]. These relevant differences in PK parameters, and thus mismatches in distribution profiles between both radiopharmaceuticals, reflect clinical observations and have also previously been reported in literature [5–10].

Individual $[^{177}\text{Lu}]\text{Lu-HA-DOTATATE}$ predictions

Our semi-physiological PK model showed that $[^{177}\text{Lu}]\text{Lu-HA-DOTATATE}$ tumor AUCs could be predicted reasonably well based on individual $[^{68}\text{Ga}]\text{Ga-HA-DOTATATE}$ scan data (with tumor AUC RPEs ranging between -40 and 28%). In addition, for tumors, individual predictions based on Bayesian parameter estimates for $[^{68}\text{Ga}]\text{Ga-HA-DOTATATE}$ outperformed population predictions for $[^{177}\text{Lu}]\text{Lu-HA-DOTATATE}$ for seven out of nine patients, confirming that diagnostic imaging provides useful information for $[^{177}\text{Lu}]\text{Lu-HA-DOTATATE}$ uptake. For the two patients where RPEs were lower for population predictions, individual uptake predictions were still accurate and differences between the individual and population approach were very small. For patient six, a clear benefit for using diagnostic imaging was shown, since the RPE based on the population model was extremely high for the tumor prediction, whereas the individual prediction (informed by diagnostic imaging) resulted in a smaller RPE and thus improved prediction (see Fig. 4). Still, this patient showed highest RPEs for both kidney and tumor, which could not be explained after looking at further patient details (such as patient characteristics, renal function and renogram scan, number and sites of metastasis, etc.). All in all, results showed that inter-individual differences in PK parameters for tumor uptake on $[^{68}\text{Ga}]\text{Ga-HA-DOTATATE}$ were informative for expected PRRT uptake. However, for kidney AUC predictions were less accurate (RPEs -53 to 41%), and even more so for absorbed doses (RPEs -58 to 82%). This could be due to the complexity of interpretation of kidney scan observations. Observed radioactivity in kidneys does not only reflect intracellular uptake, but also radioactivity in urine due to renal excretion. Especially for $[^{68}\text{Ga}]\text{Ga-HA-DOTATATE}$

Ga-HA-DOTATATE, with scan-acquisition times shortly after administration, the contribution of activity in urine is probably high. This might lead to inaccurate individual estimates of the kidney uptake parameter (k_{13}), which on its turn will result in less accurate parameter estimates for [^{177}Lu]Lu-HA-DOTATATE and thus less adequate uptake predictions. In addition, diagnostic imaging scan protocols are less stringent compared to PRRT protocols, for example, regarding supervision of patients' hydration status and co-administration of amino acid solutions. These protocol aspects could result in higher variability between patients for [^{68}Ga]Ga-HA-DOTATATE compared to PRRT with [^{177}Lu]Lu-HA-DOTATATE and these factors might contribute to the remaining mismatches in prediction of PRRT accumulation based on diagnostic imaging. Another factor that might cause uncertainty in our predictions is that population organ volumes rather than individually measured organ volumes were used. However, we assume this did not substantially impact individual model predictions. After all, we do not expect the model parameters to change with different organ volumes and potential individual differences are already taken into account in predictions by using an intra-patient prediction approach.

In general, various known and unknown external factors can influence visualization and quantification of radiopharmaceutical distributions. The physical characteristics of radionuclides and the acquisition techniques themselves may also result in (structural) differences between ^{68}Ga and ^{177}Lu imaging. For instance, noise levels in the imaging data, voxel sizes and the methods applied for quantification vary greatly between ^{68}Ga -PET/CT and ^{177}Lu -SPECT/CT, which give rise to variations in quantification of activity concentrations. Details regarding the uncertainty in image acquisition and post-processing are beyond the scope of this article, but more information can be found in previously published articles [41–43].

Results for AUC ($\mu\text{g}\cdot\text{h}/\text{L}$) and absorbed dose (Gy) clearly differed for some patients, by means that AUC RPE was accurate and absorbed dose RPE was not, or vice versa. This inconsistency was caused by the different time intervals that were used in calculations of absorbed dose compared to AUC. For AUCs, integrated concentrations over time were determined up to time of the last measurement, while for absorbed dose, the cumulative radioactivity was extrapolated up to infinity based on individual elimination rate constants. This highlights the uncertainty in dosimetry methods, where extrapolations to later time points highly impact absorbed dose calculations.

Clinical implications

A method was developed to individually predict [^{177}Lu]Lu-HA-DOTATATE PK based on single-time-point imaging with [^{68}Ga]Ga-HA-DOTATATE. Individual tumor predictions appeared less complex compared to kidney and, for tumor, it was shown that addition of information derived from diagnostic imaging improved the individual uptake predictions. However, apart from evident differences in PK parameters, there still are other factors that affect distribution differences between [^{68}Ga]Ga-HA-DOTATATE and [^{177}Lu]Lu-HA-DOTATATE.

The developed model based on data from only nine patients provides a framework for precision medicine of PRRT. Using this approach, tumor AUCs were predicted reasonably well with a RPE of approximately $\pm 30\%$. The question remains what prediction error is acceptable for applying this approach for individualized dosing in clinical care. Of

course, with nuclear imaging, day-to-day or inter-scan variability exists, which reflects a general intra-patient variability in accumulation that is observed in case nuclear imaging is repeated. We assumed this to be in the order of ~15 to 20% for [⁶⁸Ga]Ga-HA-DOTATATE PET/CT (based on clinical observations as well as results from PSMA-PET/CT imaging [44]). However, to determine maximal ranges for prediction errors, additional knowledge is warranted on variability in uptake in this population as well as the effect of tumor and kidney accumulation on efficacy and toxicity outcomes, respectively, and whether, for example, a 20% increased or decreased uptake will impact these outcomes. Possibly, prediction error requirements might even be different for kidneys (organ at risk) compared to tumors (target tissue). Once such requirements are determined, this modeling approach could help to guide individualized dosing based on expected uptake and individual deviation from the typical population. Another, somewhat similar, approach could be to individualize dosing guided based on uptake in the first PRRT cycle instead of the diagnostic imaging.

Conclusion

Semi-physiological population PK models were developed for [⁶⁸Ga]Ga-HA-DOTATATE and [¹⁷⁷Lu]Lu-HA-DOTATATE. PK parameter differences showed lower uptake rate parameters for kidney and spleen (0.29- and 0.49-fold, respectively), while the tumor uptake rate was 1.43-fold higher for [¹⁷⁷Lu]Lu-HA-DOTATATE compared to [⁶⁸Ga]Ga-HA-DOTATATE. Based on these developed models, individual Bayesian estimates for [⁶⁸Ga]Ga-HA-DOTATATE were used to calculate individual PK parameters for [¹⁷⁷Lu]Lu-HA-DOTATATE and subsequently predict [¹⁷⁷Lu]Lu-HA-DOTATATE uptake into different compartments. Although tumor AUC predictions were more accurate compared to kidney (range in relative prediction errors -40 to 28% and -53 to 41%, respectively), absorbed dose predictions were less adequate for both compartments. Many aspects, additional to PK differences, play a part in the challenging translation of [⁶⁸Ga]Ga-HA-DOTATATE to [¹⁷⁷Lu]Lu-HA-DOTATATE distribution, but this framework already confirmed that diagnostic imaging provides useful information to predict [¹⁷⁷Lu]Lu-HA-DOTATATE tumor uptake.

Abbreviations

¹⁷⁷ Lu	Lutetium-177
⁶⁸ Ga	Gallium-68
AUC	Area under the curve
B_{MAX}	Maximal binding capacity
CV	Coefficient of variation
GOF	Goodness-of-fit
ICRP	International commission on radiological protection
IIV	Inter-individual variability
NET	Neuroendocrine tumor
NLMEM	Nonlinear mixed-effects model
PBPK	Physiologically based pharmacokinetic
PK	Pharmacokinetic(s)
PRRT	Peptide receptor radionuclide therapy
RPE	Relative prediction error
RSE	Relative standard error
RUV	Residual unexplained variability
SSA	Somatostatin analogue
SSTR	Somatostatin receptor
TAC	Time-activity curve
V	Compartment volume

Supplementary Information

The online version contains supplementary material available at <https://doi.org/10.1186/s40658-023-00565-4>.

Additional file 1: Figure S1. Goodness-of-fit plots for [⁶⁸Ga]Ga-HA-DOTATATE based on the final semi-physiological population PK models. **Figure S2.** Goodness-of-fit plots for [¹⁷⁷Lu]Lu-HA-DOTATATE based on the final semi-physiological population PK models. **Figure S3.** Individual tumor and kidney predictions and observations for [¹⁷⁷Lu]Lu-HA-DOTATATE based on individual PK parameters [⁶⁸Ga]Ga-HA-DOTATATE using the final semi-physiological population PK models.

Acknowledgements

Not applicable.

Author contributions

HS, JJMAH, BjdW and ADRH contributed to the study conception and design. HS developed the models and HS, JJMAH, ADRH and TPCD discussed the modeling methodology. All authors contributed to the interpretation of the results. The first draft of the manuscript was written by HS. All authors provided critical review on previous versions of the manuscript and approved the final manuscript.

Funding

No funds, grants or other support were received.

Availability of data and materials

The datasets used for the current study are available from the corresponding author on reasonable request.

Declarations

Ethics approval and consent to participate

All procedures performed in studies involving human participants were in accordance with the ethical standards of the institutional and/or national research committee and with the 1964 Helsinki declaration and its later amendments or comparable ethical standards. Informed consent was obtained from all individual participants included in the study. The study was approved by the Institutional Review Board of the Netherlands Cancer Institute in Amsterdam, the Netherlands (IRBd21187).

Consent for publication

Not applicable.

Competing interests

The authors declare that they have no competing interests.

Received: 20 March 2023 Accepted: 24 July 2023

Published online: 24 August 2023

References

1. Ambrosini V, Kunikowska J, Baudin E, Bodei L, Bouvier C, Capdevila J, et al. Consensus on molecular imaging and theranostics in neuroendocrine neoplasms. *Eur J Cancer*. 2021;146:56–73. <https://doi.org/10.1016/j.ejca.2021.01.008>.
2. Fani M, Mansi R, Nicolas GP, Wild D. Radiolabeled somatostatin analogs: a continuously evolving class of radiopharmaceuticals. *Cancers (Basel)*. 2022. <https://doi.org/10.3390/cancers14051172>.
3. Marin JFG, Nunes RF, Coutinho AM, Zaniboni EC, Costa LB, Barbosa FG, et al. Theranostics in nuclear medicine: emerging and re-emerging integrated imaging and therapies in the era of precision oncology. *Radiographics*. 2020;40(6):1715–40. <https://doi.org/10.1148/rg.2020200021>.
4. Werner RA, Weich A, Kircher M, Solnes LB, Javadi MS, Higuchi T, et al. The theranostic promise for neuroendocrine tumors in the late 2010s: where do we stand, where do we go? *Theranostics*. 2018;8(22):6088–100. <https://doi.org/10.7150/thno.30357>.
5. Roll W, Riemann B, Schäfers M, Stegger L, Vrachimis A. 177Lu-DOTATATE therapy in radioiodine-refractory differentiated thyroid cancer: a single center experience. *Clin Nucl Med*. 2018;43(10):e346–51. <https://doi.org/10.1097/rlu.0000000000002219>.
6. Thuillier P, Maajem M, Schick U, Blanc-Beguign F, Hennebicq S, Metges JP, et al. Clinical assessment of 177Lu-DOTATATE quantification by comparison of SUV-based parameters measured on both post-PRRT SPECT/CT and 68Ga-DOTATOC PET/CT in patients with neuroendocrine tumors: a feasibility study. *Clin Nucl Med*. 2021;46(2):111–8. <https://doi.org/10.1097/rlu.00000000000003412>.
7. Ezziddin S, Lohmar J, Yong-Hing CJ, Sabet A, Ahmadzadehfar H, Kukuk G, et al. Does the pretherapeutic tumor SUV in 68Ga DOTATOC PET predict the absorbed dose of 177Lu octreotate? *Clin Nucl Med*. 2012;37(6):e141–7. <https://doi.org/10.1097/RLU.0b013e31823926e5>.
8. Sainz-Esteban A, Prasad V, Schuchardt C, Zachert C, Carril JM, Baum RP. Comparison of sequential planar 177Lu-DOTA-TATE dosimetry scans with 68Ga-DOTA-TATE PET/CT images in patients with metastasized neuroendocrine tumours undergoing peptide receptor radionuclide therapy. *Eur J Nucl Med Mol Imaging*. 2012;39(3):501–11. <https://doi.org/10.1007/s00259-011-2003-x>.

9. Öksüz M, Winter L, Pfannenbergs C, Reischl G, Müssig K, Bares R, et al. Peptide receptor radionuclide therapy of neuroendocrine tumors with (90)Y-DOTATOC: is treatment response predictable by pre-therapeutic uptake of (68)Ga-DOTATOC? *Diagn Interv Imaging*. 2014;95(3):289–300. <https://doi.org/10.1016/j.diii.2013.07.006>.
10. Huizing DMV, Aalbersberg EA, van der Hiel B, Stokkel MPM, Versleijen MWJ. Discordant uptake between diagnostic 68Ga-HA-DOTATATE PET/CT and posttherapy 177Lu-HA-DOTATATE SPECT/CT in patients with neuroendocrine tumors. *Clin Nucl Med*. 2021;46(9):e475–7. <https://doi.org/10.1097/rlu.0000000000003618>.
11. Sgourou G, Bolch WE, Chiti A, Dewaraja YK, Emfietzoglou D, Hobbs RF, et al. ICRU REPORT 96, dosimetry-guided radiopharmaceutical therapy. *J ICRU*. 2021;21(1):1–212. <https://doi.org/10.1177/14736691211060117>.
12. Lassmann M, Eberlein U, Gear J, Konijnenberg M, Kunikowska J. Dosimetry for radiopharmaceutical therapy: the European perspective. *J Nucl Med*. 2021;62(Supplement 3):735–S79. <https://doi.org/10.2967/jnumed.121.262754>.
13. Del Prete M, Buteau FA, Arsenault F, Saighi N, Bouchard LO, Beaulieu A, et al. Personalized (177)Lu-octreotate peptide receptor radionuclide therapy of neuroendocrine tumours: initial results from the P-PRRT trial. *Eur J Nucl Med Mol Imaging*. 2019;46(3):728–42. <https://doi.org/10.1007/s00259-018-4209-7>.
14. Sundlöv A, Gleisner KS, Tennvall J, Ljungberg M, Warfvinge CF, Holgersson K, et al. Phase II trial demonstrates the efficacy and safety of individualized, dosimetry-based (177)Lu-DOTATATE treatment of NET patients. *Eur J Nucl Med Mol Imaging*. 2022;49(11):3830–40. <https://doi.org/10.1007/s00259-022-05786-w>.
15. Cremonesi M, Ferrari ME, Bodei L, Chiesa C, Sarnelli A, Garibaldi C, et al. Correlation of dose with toxicity and tumour response to (90)Y- and (177)Lu-PRRT provides the basis for optimization through individualized treatment planning. *Eur J Nucl Med Mol Imaging*. 2018;45(13):2426–41. <https://doi.org/10.1007/s00259-018-4044-x>.
16. Eberlein U, Cremonesi M, Lassmann M. Individualized dosimetry for theranostics: necessary, nice to have, or counterproductive? *J Nucl Med*. 2017;58(Suppl 2):97s–103s. <https://doi.org/10.2967/jnumed.116.186841>.
17. Velikyan I. (Radio)theranostic patient management in oncology exemplified by neuroendocrine neoplasms, prostate cancer, and breast cancer. *Pharmaceuticals* (Basel). 2020. <https://doi.org/10.3390/ph13030039>.
18. Mould DR, Upton RN. Basic concepts in population modeling, simulation, and model-based drug development. *CPT Pharmacometrics Syst Pharmacol*. 2012;1:e6. <https://doi.org/10.1038/psp.2012.4>.
19. Mould DR, Upton RN. Basic concepts in population modeling, simulation, and model-based drug development-part 2: introduction to pharmacokinetic modeling methods. *CPT Pharmacometrics Syst Pharmacol*. 2013;2:e38. <https://doi.org/10.1038/psp.2013.14>.
20. Siebinga H, de Wit-van der Veen BJ, Stokkel MDM, Huitema ADR, Hendriks J. Current use and future potential of (physiologically based) pharmacokinetic modelling of radiopharmaceuticals: a review. *Theranostics*. 2022;12(18):7804–20. <https://doi.org/10.7150/thno.77279>.
21. Hartmann H, Freudenberg R, Oehme L, Zophel K, Schottelius M, Wester HJ, et al. Dosimetric measurements of (68)Ga-high affinity DOTATATE: twins in spirit—part III. *Nuklearmedizin*. 2014;53(5):211–6. <https://doi.org/10.3413/Nukmed-0667-14-05>.
22. Huizing DMV, Peters SMB, Versleijen MWJ, Martens E, Verheij M, Sinaasappel M, et al. A head-to-head comparison between two commercial software packages for hybrid dosimetry after peptide receptor radionuclide therapy. *EJNMMI Phys*. 2020;7(1):36. <https://doi.org/10.1186/s40658-020-00308-9>.
23. Aalbersberg EA, Geluk-Jonker MM, Young-Mylvaganan T, de Wit-van der Veen LJ, Stokkel MPM. A practical guide for the production and PET/CT imaging of 68Ga-DOTATATE for neuroendocrine tumors in daily clinical practice. *J Vis Exp*. 2019. <https://doi.org/10.3791/59358>.
24. van Andel L, Aalbersberg EA, Geluk-Jonker MM, Stokkel MPM, Beijnen JH, Hendriks J. The development and validation of a high performance liquid chromatography method to determine the radiochemical purity of [(177)Lu]Lu-HA-DOTA-TATE in pharmaceutical preparations. *J Chromatogr B Anal Technol Biomed Life Sci*. 2021;1171:122605. <https://doi.org/10.1016/j.jchromb.2021.122605>.
25. Reddy RP, Ross Schmidlein C, Giancipoli RG, Mauguen A, LaFontaine D, Schoder H, et al. The quest for an accurate functional tumor volume with (68)Ga-DOTATATE PET/CT. *J Nucl Med*. 2022;63(7):1027–32. <https://doi.org/10.2967/jnumed.121.262782>.
26. Siebinga H, de Wit-van der Veen BJ, Beijnen JH, Dorlo TPC, Huitema ADR, Hendriks J. A physiologically based pharmacokinetic model for [(68)Ga]Ga-(HA-)DOTATATE to predict whole-body distribution and tumor sink effects in GEP-NET patients. *EJNMMI Res*. 2023;13(1):8. <https://doi.org/10.1186/s13550-023-00958-7>.
27. Basic anatomical and physiological data for use in radiological protection: reference values. A report of age- and gender-related differences in the anatomical and physiological characteristics of reference individuals. *ICRP Publication 89*. *Ann ICRP*. 2002;32(3–4):5–265.
28. Reubi JC. Peptide receptors as molecular targets for cancer diagnosis and therapy. *Endocr Rev*. 2003;24(4):389–427. <https://doi.org/10.1210/er.2002-0007>.
29. Hardiansyah D, Attarwala AA, Kletting P, Mottaghy FM, Glatting G. Prediction of time-integrated activity coefficients in PRRT using simulated dynamic PET and a pharmacokinetic model. *Phys Med*. 2017;42:298–304. <https://doi.org/10.1016/j.ejmp.2017.06.024>.
30. Jimenez-Franco LD, Glatting G, Prasad V, Weber WA, Beer AJ, Kletting P. Effect of tumor perfusion and receptor density on tumor control probability in (177)Lu-DOTATATE therapy: an in silico analysis for standard and optimized treatment. *J Nucl Med*. 2021;62(1):92–8. <https://doi.org/10.2967/jnumed.120.245068>.
31. Puszkial A, Bauriaud-Mallet M, Bourgeois R, Dierickx L, Courbon F, Chatelut E. Evaluation of the interaction of amino acid infusion on (177)Lu-Dotatate pharmacokinetics in patients with gastroenteropancreatic neuroendocrine tumors. *Clin Pharmacokinet*. 2019;58(2):213–22. <https://doi.org/10.1007/s40262-018-0674-1>.
32. Lambert M, Dierickx L, Brillouet S, Courbon F, Chatelut E. Comparison of two types of amino acid solutions on (177)Lu-Dotatate pharmacokinetics and pharmacodynamics in patients with metastatic gastroenteropancreatic neuroendocrine tumors. *Curr Radiopharm*. 2022;15(2):164–72. <https://doi.org/10.2174/1874471015666211228123525>.
33. Beaugerard JM, Hofman MS, Kong G, Hicks RJ. The tumour sink effect on the biodistribution of 68Ga-DOTA-octreotate: implications for peptide receptor radionuclide therapy. *Eur J Nucl Med Mol Imaging*. 2012;39(1):50–6. <https://doi.org/10.1007/s00259-011-1937-3>.

34. Siebinga H, Heuvel JO, Rijkhorst EJ, Hendriks J, de Wit-van der Veen BJ. The impact of peptide amount on tumor uptake to assess PSMA receptor saturation on (68)Ga-PSMA-11 PET/CT in patients with primary prostate cancer. *J Nucl Med*. 2023;64(1):63–8. <https://doi.org/10.2967/jnumed.122.264101>.
35. Lubberink M, Wilking H, Ost A, Ilan E, Sandstrom M, Andersson C, et al. In vivo instability of (177)Lu-DOTATATE during peptide receptor radionuclide therapy. *J Nucl Med*. 2020;61(9):1337–40. <https://doi.org/10.2967/jnumed.119.237818>.
36. Siebinga H, de Wit-van der Veen BJ, Beijnen JH, Stokkel MPM, Dorlo TPC, Huitema ADR, et al. A physiologically based pharmacokinetic (PBPK) model to describe organ distribution of (68)Ga-DOTATATE in patients without neuroendocrine tumors. *EJNMMI Res*. 2021;11(1):73. <https://doi.org/10.1186/s13550-021-00821-7>.
37. Bauer RJ. NONMEM tutorial part I: description of commands and options, with simple examples of population analysis. *CPT Pharmacometrics Syst Pharmacol*. 2019;8:525–37. <https://doi.org/10.1002/psp4.12404>.
38. Bolch WE, Eckerman KF, Sgouros G, Thomas SR. MIRD pamphlet No. 21: a generalized schema for radiopharmaceutical dosimetry—standardization of nomenclature. *J Nucl Med*. 2009;50(3):477–84. <https://doi.org/10.2967/jnumed.108.056036>.
39. Andersson M, Johansson L, Eckerman K, Mattsson S. IDAC-Dose 2.1, an internal dosimetry program for diagnostic nuclear medicine based on the ICRP adult reference voxel phantoms. *EJNMMI Res*. 2017;7(1):88. <https://doi.org/10.1186/s13550-017-0339-3>.
40. de Jong M, Rolleman EJ, Bernard BF, Visser TJ, Bakker WH, Breeman WA, et al. Inhibition of renal uptake of indium-111-DTPA-octreotide in vivo. *J Nucl Med*. 1996;37(8):1388–92.
41. Finocchiaro D, Gear JI, Fioroni F, Flux GD, Murray I, Castellani G, et al. Uncertainty analysis of tumour absorbed dose calculations in molecular radiotherapy. *EJNMMI Phys*. 2020;7(1):63. <https://doi.org/10.1186/s40658-020-00328-5>.
42. Gear JI, Cox MG, Gustafsson J, Gleisner KS, Murray I, Glatting G, et al. EANM practical guidance on uncertainty analysis for molecular radiotherapy absorbed dose calculations. *Eur J Nucl Med Mol Imaging*. 2018;45(13):2456–74. <https://doi.org/10.1007/s00259-018-4136-7>.
43. Li T, Ao ECI, Lambert B, Brans B, Vandenberghe S, Mok GSP. Quantitative imaging for targeted radionuclide therapy dosimetry—technical review. *Theranostics*. 2017;7(18):4551–65. <https://doi.org/10.7150/thno.19782>.
44. Olde Heuvel J, de Wit-van der Veen BJ, Donswijk ML, Slump CH, Stokkel MPM. Day-to-day variability of [(68)Ga]Ga-PSMA-11 accumulation in primary prostate cancer: effects on tracer uptake and visual interpretation. *EJNMMI Res*. 2020;10(1):132. <https://doi.org/10.1186/s13550-020-00708-z>.

Publisher's Note

Springer Nature remains neutral with regard to jurisdictional claims in published maps and institutional affiliations.

Submit your manuscript to a SpringerOpen[®] journal and benefit from:

- Convenient online submission
- Rigorous peer review
- Open access: articles freely available online
- High visibility within the field
- Retaining the copyright to your article

Submit your next manuscript at ► [springeropen.com](https://www.springeropen.com)
